EUROPEAN ORGANIZATION FOR NUCLEAR RESEARCH
European Laboratory for Particle Physics

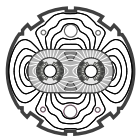

Large Hadron Collider Project

LHC Project Report 44

QUENCH LEVELS AND TRANSIENT BEAM LOSSES IN LHC MAGNETS

J.B. Jeanneret[*,§], D. Leroy[†], L. Oberli[†], T. Trenkler[‡]

Abstract

The last evaluation of quench levels related to transient beam losses was done in 1987 [1]. The subject is reevaluated with a more detailed approach of the thermodynamics of the superconducting cables in response to a transient heat load associated to beam losses.

[*]CERN–SL Division
[†]CERN–LHC Division
[‡]Formerly CERN–SL Division, now at Siemens-Matsushita OHG, Deutschlandsberg,Austria
[§]jbj@mail.cern.ch

Administrative Secretariat
LHC Division
CERN
CH-1211 Geneva 23
Switzerland

Geneva, 29 July 1996

1 INTRODUCTION

The last evaluation of quench levels related to transient beam losses was done in 1987 [1]. The subject is reevaluated with a more detailed approach of the response of the superconducting cables to a transient heat load associated to beam losses.

Our conclusions do not depart substantially from the former study, but we nevertheless propose updated levels of quenching and a more precise time-scale associated to different levels of transient losses.

After a brief summary of the results of hadronic shower simulations in LHC magnets (section 2), the temperature dependent specific heat of the different elements of the cables are given in section 3. We discuss the structure of the superconducting cables and some associated thermodynamical time constants in section 4. The number of protons lost in a short time necessary to induce a quench is computed in section 5, while section 6 contains a reminder about steady state losses.

By comparing the numbers given in Sections 5 and 6 we see that the allowed transient losses before quenching are only related to the enthalpy reserve of the wires, supplemented in some conditions by the heat reserve of the helium statically present locally in the cable.

2 HADRONIC SHOWERS

The energy of a proton impacting on matter is dissipated through two processes.

- The proton interacts on a nucleus and produces many secondary particles, which later also interact, and so on, until the residual energy per particle is too small to create additional ones. In ordinary metals (iron or copper) the average distance between two interactions is $l \approx 15cm$ and the effective length of the showers is $L \approx 1m$, with a tail expanding up to $\approx 10L$. The result of this process is called a hadronic shower. It is combined to electromagnetic showers through the decay of neutral pions into two photons.
- Charged particles ionise atoms along their path. The excited electrons release their kinetic energy to the lattice, or by emitting photons in the atomic range of energy, which are absorbed and converted to phonons locally.

Finally almost all the incident energy is converted to heat. The spatial distribution of heat deposition cannot be computed analytically with a good accuracy, but good Monte-Carlo programs exist today. In the present work we use simulations done with the program CASIM [2], in which we introduced the essential of the geometry of a LHC magnet, as well as the field map at both the injection and top energy nominal fields. This study has already been described [3]. The results are consistent with those obtained in a separate analysis done with the program FLUKA [4, 5, 6]. We simulated the impact of protons on a single location of the beam screen of a LHC dipole. The transverse geometry of the dipole is shown in Figure 1. The angle of attack was the betatronic angle $x' = 0.24$mrad at the location of impact. Different parameters were varied, with little effect on the results[3].

For simplicity, we used Iron instead of the real mixing of Cu/NbTi of the coils. The nuclear absorption and radiation lengths of Iron are $\approx 10\%$ smaller than those one of Copper, almost compensating the weak contribution to shower development of the insulation material and the helium, which occupy together $\approx 10\%$ of the volume of the coil (see Section 3).

An ideal simulation would provide the three-dimensional density of energy deposition $d^3E/drd\varphi ds$, with r the transverse radial coordinate, φ the transverse azimuth and s the longitudinal coordinate. In practice, computer time limitations made us choose quite

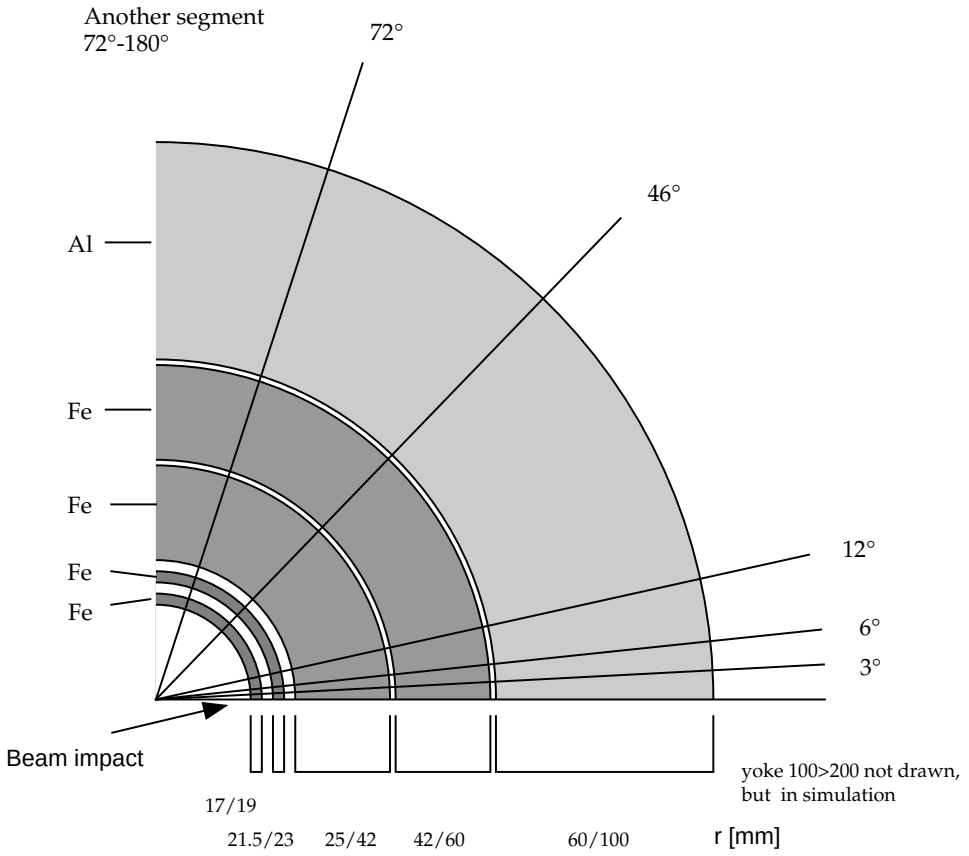

Figure 1: The description of the dipole used in the hadronic shower simulation with the Casim program. The beam impacts on the beam screen with a grazing angle of 0.24mrad and in the horizontal plane. The energy deposition is scored in every cell delimited by the radial and the azimuthal lines

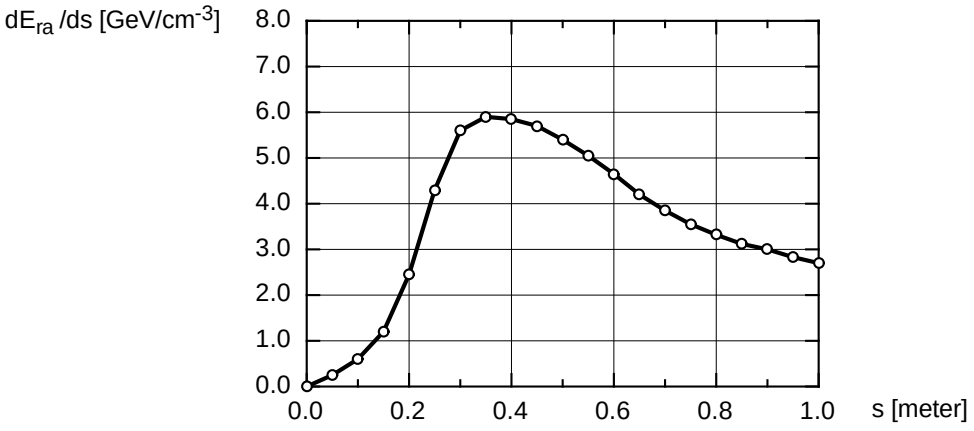

Figure 2: The longitudinal energy deposition in the most exposed cable at top energy. The simulated data have been smoothed for better presentation. The impact point of the protons on the beam screen is at $s = 0$

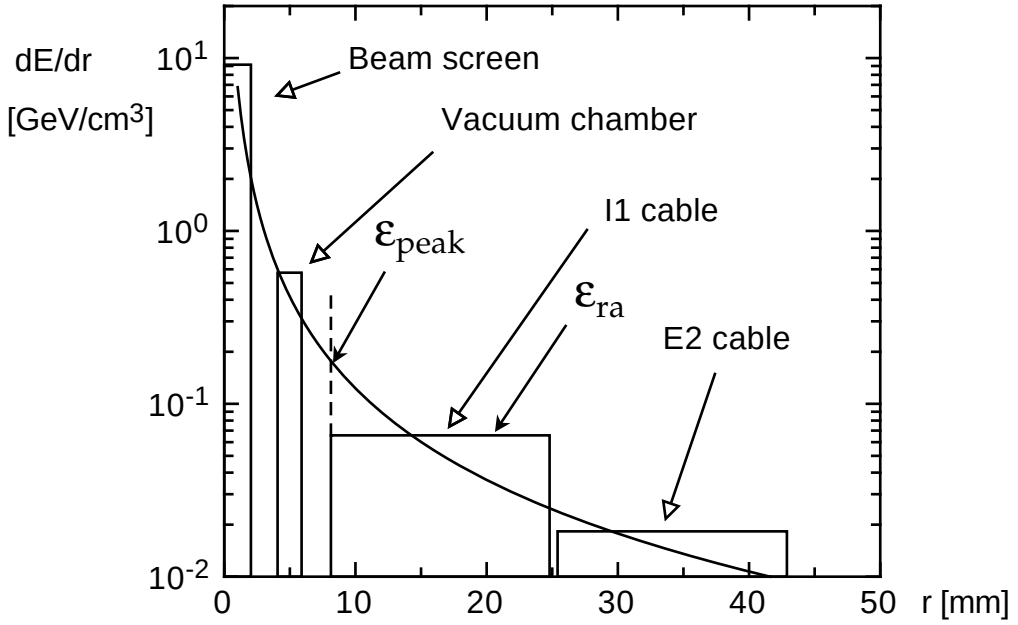

Figure 3: The maximum radial energy density along the most exposed azimuth

large recording cells. In the coil, the basic cell for recording the deposition of energy was the transverse section of the cables (see Figure 1) with a longitudinal segmentation of 100mm. Therefore, we only get directly the average energy density ε_{ra} in the transverse cells, i.e. for the cables, the average density over their section (see Figure 2 for this function along s in the most exposed cable). In order to estimate the peak density deposition in the cable, a sharper distribution is needed. An empirical fit of the radial dependence of the maximum energy deposition per unit volume in the beam screen, the vacuum chamber and the two layers of cables with a power law $\varepsilon(r) = Ar^{-n}$ allowed to deduce the maximum transverse deposition of energy in smaller areas of cable with an adequate precision. The constraints on $\varepsilon(r)$ are to reproduce correctly the different ε_{ra} values (see Figure 3). The origin of r is at the inner side of the beam screen, where the beam touches first. The fitted exponents are $n = 1.76$ at injection and $n = 1.15$ at top energy. The function $\varepsilon(r)$ in GeV/cm^{-3} is the maximum deposition of energy at every radial value r, independent of the longitudinal coordinate s.

Beyond the beam screen and the vacuum chamber, the conductor closest to the impact point receives the maximum energy deposition of heat at both injection and top energy. If a beam loss occurs during a short time ($< 3000\mu$s, see Section 4.1), the heat does not migrate substantially in the cable even transversely. If the time dilution is large enough, the heat can diffuse transversely in the Cu/NbTi wires. In the first case, the quench limit occurs at the edge of the cable facing the beam. The maximum energy density deposited per proton lost at that radial position is called ε_{peak} and is deduced from the radial fit discussed above. In the second case, the radial (or transverse) average value, called ε_{ra} must be used instead. With the fit of the exponent n, we get $\varepsilon_{peak}/\varepsilon_{ra} = 2.7$ at injection and $\varepsilon_{peak}/\varepsilon_{ra} = 1.8$ at top energy.

The CASIM simulation was done with a radial cable size of 17mm, now changed to 15mm. By integrating the power laws, a difference of 6% (injection) and 8% (top) is computed between the two kinds of inner cable for the variable ε_{ra} (see below and

Table 1: Maximum energy densities, peak and radial average, local (per proton), and distributed (per proton/m), deposited in the most exposed superconducting cable of a dipole. The original simulation at top energy was made at 8TeV. All ε values are given both in GeV (top) and in Joule (bottom) units.

	$\varepsilon_{peak,local}$	$\varepsilon_{ra,local}$	$\varepsilon_{peak,dist}$	$\varepsilon_{ra,dist}$
Beam Energy	$[GeV/cm^3]$	$[GeV/cm^3]$	$[GeV \cdot m/cm^3]$	$[GeV \cdot m/cm^3]$
Injection .45TeV	0.24	0.085	0.24	0.085
Top 7TeV	10.8	5.5	7.9	4.0
	$[J/cm^3]$	$[J/cm^3]$	$[J \cdot m/cm^3]$	$[J \cdot m/cm^3\ ]$
Injection .45TeV	$3.8 \cdot 10^{-11}$	$1.4 \cdot 10^{-11}$	$3.8 \cdot 10^{-11}$	$1.4 \cdot 10^{-11}$
Top 7TeV	$1.7 \cdot 10^{-9}$	$0.88 \cdot 10^{-9}$	$1.3 \cdot 10^{-9}$	$0.64 \cdot 10^{-9}$

Table 1). To correct for the decrease of the top energy from 8TeV to 7TeV, the maximum energy deposition ε_{peak} and ε_{ra} are decreased by 12%.

At top energy, $\varepsilon_{ra} = dE_{ra}^{max}(s)/ds$ is reached at $s \approx 350$mm. The values ε_{ra} and ε_{peak} are given in Table 1.

Also shown in Table 1 is the energy density ε_{dist} per proton$\cdot$m^{-1} related to a longitudinally distributed loss of protons in the most exposed cable (here I1), spread over a distance longer than the length of the shower.

The value ε_{dist} is obtained by convoluting the curve of Figure 2 with a long rectangular s-distribution. For a longitudinally continuous density of protons falling on the beam screen n_{dist} (in units [protons/m]), the continuous energy density is (using $e(s) = dE/ds$)

$$g_{dist} = n_{dist} \cdot \int_0^\infty e(s)\ ds = n_{dist}\varepsilon_{dist} \tag{1}$$

while the same density is reached in the case of a local loss of n_{local} (in units [proton]) as

$$g_{local} = n_{local} \cdot e_{max} \tag{2}$$

with e_{max} being either ε_{peak} or ε_{ra}. Equating the left quantities for equal maximum density of energy, we get

$$\frac{\varepsilon_{dist}}{e_{max}} = \frac{n_{local}}{n_{dist}} = \int \frac{e(s)\ ds}{\varepsilon_{local}} = L_{eff}. \tag{3}$$

A quench occurs in both cases when $e \cdot n$ reaches the critical energy (see below) and therefore

$$\varepsilon_{dist} = e_{max} \cdot L_{eff}. \tag{4}$$

L_{eff} is the effective length of the shower along the most exposed cable.

L_{eff} is numerically integrated with the Monte-Carlo data as $L_{\text{injection}} = 1.0$m and $L_{\text{top energy}} = 0.7$m. It has been verified that the ratio $\varepsilon_{peak}/\varepsilon_{ra}$ is not notably modified when the losses are distributed.

Critical energy density for quench

The density ε of energy per proton (either local or distributed longitudinal loss) is directly related to the quench level in the case of transient losses. When the time duration of the loss is fast compared to a given thermal diffusion time constant in the s.c. coils, the number of protons n_q to induce a quench is

$$n_q = \frac{\Delta Q_c}{\varepsilon} \tag{5}$$

where ΔQ_c is the amount of heat per unit volume which is necessary to raise the temperature to its critical value T_c. Different ε values are given in Table 1. It will be seen in Section 5 that both ΔQ_c and ε depend on the duration δt of a transient loss thus making n_q dependent on δt.

3 SPECIFIC HEAT AND ENTHALPY IN SOLID ELEMENTS

We need to know the specific heat as a function of temperature for three kinds of solid materials, i.e. in

- Copper
- Superconducting NbTi
- The insulation material of the wire

The main ingredient for the specific heat of solids is related to vibrations of the lattice (or phonons) and to the free electrons if a metal is considered. This is well described by the theory of Debye. This theory uses a fixed lattice constant and therefore allows the calculation of the specific heat $c_v(T)$. In our case the wires are almost free to expand locally since they are surrounded by liquid helium and we shall use $c_p(T)$. But in a limited range of temperature $c_p = c_v$ to a very good approximation.

We readily make use of the existing theory and data to fix the specific heat $c(T)$ of copper and of the insulation material. The case of NbTi in superconducting state requires a bit more attention.

3.1 CRITICAL TEMPERATURES

In the operating conditions of the dipoles, the critical temperatures are given in Table 2. These values shall be understood as the ones at which a quench will occur. But the stored beams will suffer from magnetic field instabilities at temperatures slightly lower than the critical ones. Realistic estimates for quench limits shall therefore make room for some contingency.

3.2 SPECIFIC HEAT OF COPPER

At low enough temperature the specific heat of ordinary metals (here copper) can be accurately parametrised by

$$c_{Cu}(T) = c_v = \gamma_{Cu} \cdot T + \alpha_{Cu} \cdot T^3 \tag{6}$$

The linear term is related to conduction electrons and the cubic one to the lattice waves or phonons. The third power of T is a low energy Taylor development of the formula obtained from the theory of Debye[15]. For copper[14],

$$\gamma_{Cu} = 9.686 \cdot 10^{-2} \mathrm{m}Jcm^{-3}K^{-2} \qquad \alpha_{Cu} = 6.684 \cdot 10^{-3} \mathrm{m}Jcm^{-3}K^{-4} \tag{7}$$

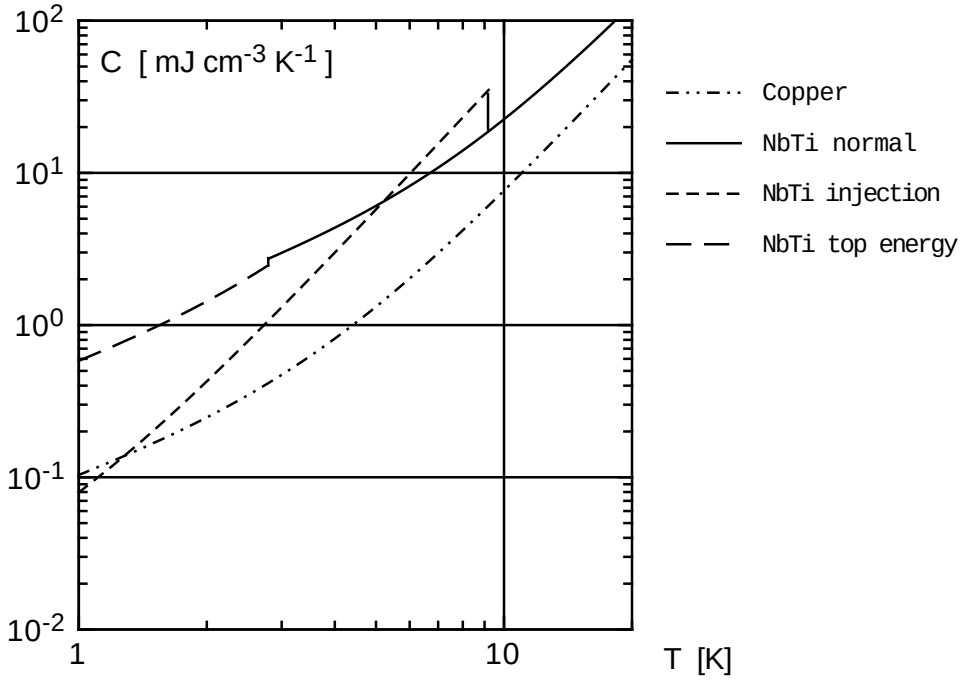

Figure 4: The specific heat of NbTi and copper

3.3 SPECIFIC HEAT OF NbTi

This section is a summary of the work by Elrod, Miller and Dresner[16] and by Lubell[17]. In the superconducting state of a metal, the conduction electrons at the top of the Fermi sea are no more free to move independently. They aquire a compact behaviour, itself compactly coupled to the phonons. For this reason, it can be shown that the linear term of $c(T)$ disappears at null magnetic field, while the cubic term is increased when compared to the normal state of the same material. Further, $c(T)$ contains a new term, linear with both T and the magnetic field B, which is another consequence of the special behaviour of the conduction electrons. Beyond the critical temperature at a given field, the normal shape of $c(T)$ reappears.

All these phenomena require a thorough theoretical investigation, well beyond the scope of the present document. It is enough to see in [16] that the above facts are clearly borne out experimentally. Elrod et al. [16] have compared their results to other measurements and they observe relative differences of the order of 20%, while giving convicing arguments for finding their own values to be the most precise set. We therefore use their parametrisation for the s.c state of NbTi.

$$c_{NbTi}(T) = c_v = \gamma_{NbTi} \cdot \frac{B}{B_{c2(0)}} T + \alpha_{NbTi} \cdot T^3 \tag{8}$$

where

$$\gamma_{NbTi} = 0.87 \mathrm{m} J cm^{-3} K^{-2} \tag{9}$$

$$\alpha_{NbTi} = \beta_{NbTi} + 3\gamma_{NbTi}/T_c = 4.464 \cdot 10^{-2} \mathrm{m} J cm^{-3} K^{-4} \tag{10}$$

with

$$\beta_{NbTi} = 1.38 \cdot 10^{-2} \mathrm{m} J cm^{-3} K^{-4} \tag{11}$$

and

$$T_c = T_c(B=0) = 9.2K \qquad , \qquad B_{c2(0)} = B_{c2}(T=0) = 14\text{T} \tag{12}$$

All the numerical values are deduced from [16].

Above (B_c,j_c), in the normal state we use

$$c(T) = \gamma_{NbTi}T + \beta_{NbTi}T^3 \tag{13}$$

with β and γ as above.

3.4 SPECIFIC HEAT OF THE INSULATION MATERIAL

The insulation material is basically made of Kapton for which the specific heat is $c(4K) = 3.6 \cdot 10^{-3}\text{mJcm}^{-3}\text{K}^{-1}$ and $c(10K) = 26 \cdot 10^{-3}\text{mJcm}^{-3}\text{K}^{-1}$ [18]. These values are very close to the specific heat of NbTi. For its small relative volume (see Table 3) and its much smaller heat conductivity than the metals, the insulation material has little impact on transient losses.

3.5 ENTHALPY RESERVE OF THE WIRE

Between the steady temperature of the bath, $T_1 = 1.9\text{K}$ and the critical temperature of quenching $T_2 = T_c(B,j)$, the enthalpy difference ΔH of the wires is obtained by adding $c(T)$ of copper and NbTi with the adequate weight and by integrating between T_1 and T_2. We get

$$H_{wire}(T) = a(B)T^2 + bT^4 + const \tag{14}$$

with

$$a(B) = \frac{1}{2(1+f)}(f\gamma_{Cu} + \gamma_{NbTi}\frac{B}{B_{c2(0)}}) \qquad and \qquad b = \frac{1}{4(1+f)}(f\alpha_{Cu} + \alpha_{NbTi}) \tag{15}$$

where f = 1.6 (Section 4). Numerically,

$$a(B) = 2.98 \cdot 10^{-2} + 0.167B/B_{c2(0)} \quad \text{and} \quad b = 5.39 \cdot 10^{-3}. \tag{16}$$

The enthalpy reserve of the wire $\Delta H_{wire} = H_{wire}(T_2) - H_{wire}(T_1)$ are given in Table 2. $T_1 = 1.9\text{K}$ is the steady temperature of the helium bath and T_2 is the critical temperature T_q.

3.6 HEAT RESERVE IN HELIUM

The heat ΔQ which is necessary to reach a temperature T_2 in helium, starting at the temperature of the bath $T_1 = 1.9\text{K}$ must be evaluated differently in two temperature intervals. In the liquid phase, but only up to the transition between helium II and I at $T_1 = 2.168\text{K}$, $c_p = c_v = c(T)$ [20]. Therefore [20]

$$\Delta Q_\lambda = \int_{T_1}^{T_\lambda} c(T)dT = 1.6 \text{ Jg}^{-1} = 233 \text{ mJcm}^{-3}. \tag{17}$$

Above T_λ, in helium I and in the gaseous state c_p and c_v differ substantially [21] and this domain of temperature requires additional thoughts. The sole quantity which depends on nothing is the latent heat of evaporation. The helium inside the cable is confined

Table 2: The enthalpy reserve of the superconducting wire, the helium and the cable. The fractional volume of helium is assumed to be 5%, see Table 3. T_q is the temperature at which the superconducting state is lost for the operating field B_o. The steady temperature in the abscence of beam losses is the one of the helium bath $T_{\rm bath} = 1.9K$. For ϕ_V and τ, see Section 4.2.

Energy [GeV]	B_o [T]	T_q [K]	Heat reserve [mJcm^{-3}]			ϕ_V [Wcm^{-3}]	τ_{He} [s]	τ_{metal} [s]
			ΔH_{wire}	ΔQ_{He}	ΔQ_{cable}			
450	0.56	9	38	313	351	8	$4.4 \cdot 10^{-2}$	$6 \cdot 10^{-3}$
7000	8.65	2.8 [a)]	0.8	29.0	29.8	4	$8 \cdot 10^{-3}$	$3 \cdot 10^{-3}$

[a)] T_q increases by $\sim 0.1K$ if B_o decreases by $0.1T$. The nominal operational field is at present $B_o = 8.4T$ and therefore $T_q \approx 3.0K$ (these parameters are still subject to small changes). With these updated values, the heat reserve at top energy become $\Delta H_{wire} = 1.07$ (+34%) and $\Delta Q_{He} = 35$ (+22%)

into capillaries delimited by the wires. They have a typical transverse dimension of $d \approx 0.3mm$. A shower develops longitudinally over $L \approx 1m$. The speed of sound in helium is $v \approx 5200m/s$ in our domain of temperature [20]. A strong underestimation of the time needed for the heat to move over a distance $L/2$ is $\Delta t = L/2v = 2\text{ms} \approx 200$beam turns. We deduce that the process occurs at fixed volume whenever fast losses are considered. In addition there is no significant exchange through the insulation of the cable. This is obvious when comparing the allowed rate of transient losses (Section 5) to what is allowed in steady state (Section 6). Therefore, once the heat deposit is ended, the process is adiabatic and develops at fixed volume. The allowed heat deposition is then expressed by

$$\Delta Q_2 = \int_{T_\lambda}^{T_2} c_v(T) dT \tag{18}$$

In this case, ΔQ can no more be identified to enthalpy which is a thermodynamical potential when p =constant. Using the data of McCarty [20, 21] and the density $\rho = 0.147\text{gcm}^{-3}$, we get $\Delta Q = \Delta Q_\lambda + \Delta Q_2 = 6.3\text{Jcm}^{-3}$ for $T_2 = 9K$ and $\Delta Q = 0.58\text{Jcm}^{-3}$ for $T_2 = 2.8K$ (Table 2). The heat reserve ΔQ_{He} in Table 2 is multiplied by the fractional volume of 5% of helium in the cable.

4 COIL STRUCTURE AND THERMAL CONSTANTS

A schematic cut view of a superconducting cable is shown in figure 5. The structure of the cables is described in [9] and [10]. The wires are made of NbTi filaments inserted inside a Copper matrix. The helium occupies the space between the wires or between the wires and the insulator. The fractional volume of the different components of the cable are given in Table 3, from which we derive

$$f = \frac{\Delta V_{Cu}}{\Delta V_{NbTi}} = 1.6 \tag{19}$$

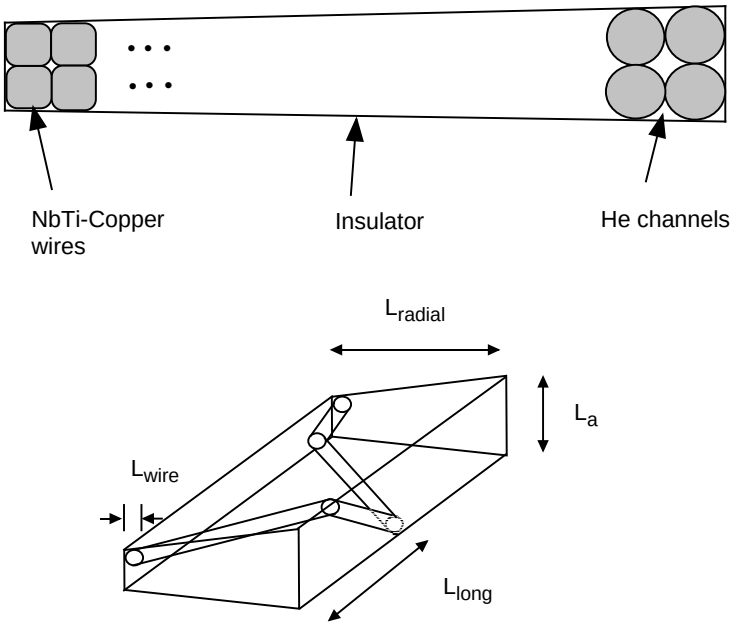

Figure 5: The simplified cut view of a cable (top) showing the inhomogeneous density of helium. The distances of the bottom figure are given in Table 4.

Table 3: Fractional volumes in the s.c cables of the LHC magnets

Material	$\Delta V/V$ [%]	ρ[gcm^{-3}]
Helium	5.0	0.147
Insulation material	3.0	$\approx$ 1.4
Cu	56.6	8.96
NbTi	35.4	6.0

Table 4: Temperature decay time constants in the cable at injection ($T \leq 9$K) and at top energy ($T \leq 4$K). The transverse time constants depend on the resistance at the surface of the wires. The contribution of helium is excluded here (see Section 4.2).

	size L [cm]	τ [μs] injection	τ [μs] top energy
Wire radius r	0.05	$\tau_{wire} = 8$	$\tau_{wire} = 4$
Small transverse L_a	0.17	$\tau_a \geq 300$	$\tau_a \geq 150$
Large transverse L_{radial}	1.5	$\tau_{radial} \geq 20000$	$\tau_{radial} \geq 10000$
Longitudinal L_{long}	2.75	$\tau_{long} = 6000$	$\tau_{long} = 3000$

The thermal contact between two cables is poor. Heat transport out of the cable is dominated by the flow of helium through the insulator. This has a marginal contribution when considering transient losses ($dt \ll 1s$). This is quantitatively demonstrated by comparing the transient quench levels (section 5) to the steady state allowed rates (section 6).

A quench occurs in a cable when enough heat is deposited locally for the temperature to grow above the critical one (Section 3.1 and Table 2). If the deposition of heat is not homogeneous, it will diffuse in the cable and also be transferred from the wires to the helium stored in the cable. In section 4.1 we estimate some diffusion time constant in the conductor. In section 4.2 the time constant for the transfer of heat between the wires and the helium is evaluated. These time constants will allow to fix which fraction of the heat reserve ΔQ_c of the cable and which ε shall be used in (5) for a given time scale.

4.1 HEAT DIFFUSION IN WIRES

The conduction of heat inside the cables cannot be reduced to the case of an homogeneous mixing of Cu and NbTi. Transversely, the resistance of contact between adjacent wires dominates and might be deliberately increased for better field quality of the magnets. An indicative value for direct transverse diffusion is given in Table 4. Longitudinally, a microscopic model of heat diffusion in the wire reveals substantial differences between the real structure and the homogeneous equivalent. This study is continuing. At top energy ($T < 4$K), a good approximation is presently deduced from this model [8] as

$$\tau \approx 364 \cdot L^2 \qquad [\mu\text{s}, \text{cm}] \tag{20}$$

for a sample of length L and the range of temperature gradients corresponding to the heat deposition discussed in section 2 (see Figure 3). At injection, where the temperature shall rise to $T \sim 9$K, the constant in (20) must be approximately doubled [8]. The longitudinal characteristic distance is determined to be close to one fourth of the period of rotation of the wire inside the cable (see Figure 5). The corresponding τ_{long} time (see Table 4) fixes the time-scale needed to equalise the temperature between the inner and the outer edge of the cable, and is therefore also a transverse time constant. It will be called τ_{metal} below ($\tau_{metal} = \tau_{long}$).

4.2 HEAT TRANSMISSION BETWEEN THE WIRE AND THE HELIUM

If the flux of heat between the wire and the helium is large, a gap of temperature ΔT_{gap} appears at their interface, and the process saturates in the so-called 'film boiling' regime. At $T_{gap} \sim 1K$, the surface ϕ_S flux saturates at $\phi_S \sim 1W/cm^2$ and the temperature then immediately rises to $T \sim 10K$ [12]. Therefore the maximum allowed flux shall be $\phi_{S,max} \approx 1W/cm^2$ at injection, and $\phi_{S,max} \approx 0.5W/cm^2$ at top energy to stay below $T = 2.8K$ (see Table 2 for critical temperatures).

The flux of heat from the wire to the helium per unit volume ϕ_V is the product of the flux per unit of surface of contact copper-helium ϕ_S, by the surface of contact per unit volume of conductor S_V. With a wire of radius $r = 0.05cm$ and an expected relative surface of contact of $f_{contact} \sim 20\%$ [8], $S_V = f_{contact}(2\pi rl)/(\pi r^2 l) = 2f_{contact}/r = 8cm^2/cm^3 = 8cm^{-1}$ and $\phi_V = \phi_S \cdot S_V$. The numerical values are given in Table 2. This limitation of flux is an an additional time constraint, in that sense that to make full use of the heat reserve of the helium, the heat flux per unit volume shall not be larger than ϕ_V. The time constant is computed as

$$\tau_{He} = \Delta Q_{He}/\phi_V. \tag{21}$$

The quantity ΔQ_{He} is given in Section 3.6.

5 LEVEL OF QUENCHING FOR TRANSIENT LOSSES

In Section 2, the level of quenching was defined by a number of protons n_q lost locally as

$$n_q = \frac{\Delta Q_{critical}}{\varepsilon}. \tag{22}$$

The maxima ε of the energy deposition per proton and per unit volume in the s.c coil are defined in Table 1. We must consider three cases, for which both ε and ΔQ differ.

a) The duration of the pulse of loss is very short, or $\delta t \ll \tau_{metal} = \tau_{long}$ (see Section 5.1). Then the temperature does not equalise transversely between the inner and the outer edge of the cable (Section 4) and in addition the helium does not contribute ($\tau_{He} > \tau_{long}$, see Table 2). The energy deposition in the most exposed wire shall be considered and then

$$\Delta Q_{critical} = \Delta H_w \qquad \text{and} \qquad \varepsilon = \varepsilon_{peak}. \tag{23}$$

b) The duration of the loss is close to $\delta t \leq \tau_{metal}$ (see Section 4). Then the temperature increases in the wire with no substantial heat transfer to the helium but diffuses in the wire across the section of the cable. Once the critical temperature T_c is reached, the quench occurs before the heat transfer to the helium helps to maintain the temperature low enough below T_c. In this case

$$\Delta Q_{critical} = \Delta H_w \qquad \text{and} \qquad \varepsilon = \varepsilon_{ra}. \tag{24}$$

c) The duration of the loss is close to than $\delta t \approx \tau_{He}$ but remains finite. Then an equilibrium of temperature occurs between the interior of the wire and the helium which is present in the cable . Therefore, ΔQ_c will be

$$\Delta Q_{critical} = \Delta Q_{cable} = \Delta H_w + \Delta Q_{He} \qquad \text{and} \qquad \varepsilon = \varepsilon_{ra}. \tag{25}$$

Table 5: Time scale for beam compared to time constants related to heat transfer in the superconducting cables.

	Beam	$\Delta t[\mu s]$	Cables	$\tau[\mu s]$	Beam turns
Fast losses			Filament	$\leq 10^{-3}$	
	Single bunch	$5 \cdot 10^{-3}$			
			Wire radius	4	
	One SPS batch	6			
	One LHC turn	89			≤ 1
Medium range losses			Cable (metal)		
			- Injection	6000	70
			- Top	3000	35
			Exhaust of He heat reserve		
			- Injection	$4.4 \cdot 10^4$	500
			- Top	$8 \cdot 10^3$	90
Slow losses	RF losses at ramping	$\simeq 2 \cdot 10^5$			2200
	Steady losses	∞			∞

At both injection and top energy, the limited heat flow from the metal to the helium fixes the longest time-scale (see Table 2). A summary of the quench limits is given in Table 6 for local or longitudinally distributed losses and the three time scales considered here. The two sets of values are correlated by the factor $\varepsilon_{distributed}/\varepsilon_{local}$ of Table 1.

If a loss lasts $\delta t < \tau$ (either metal or helium), the number of protons leading to quench of Table 6 shall be reduced by the ratio $\delta t/\tau$ (for an approximate result).

The numbers in Table 6 must be considered with some care. As an example, the peak magnetic field is somewhat larger than the nominal value used to compute the critical temperature. The thickness of both the vacuum chamber and the beam screen are not yet finalised, thus the density of energy deposition in the cable might change. A margin of $\pm 50\%$ is certainly not exagerately safe.

5.1 A SINGLE BUNCH AT INJECTION

At the starting-up of LHC, a single bunch will be injected. The bunch might touch the vacuum chamber if the orbit of the beam is bad beyond the collimation system. The duration of the loss will be $\delta t < 5\text{ns} \ll \tau_{metal}$. As for choosing the longitudinal distribution of the loss, we shall discard the case where the loss occurs on a step of the vacuum chamber, on the grounds that such steps should be avoided for other reasons and anyway it is unlikely that the trajectory will have just the right phase to produce a full loss at that location.

What is most probable is a loss with an angle of incidence nearly equal to the betatronic angle at some locations, usually where $\beta = \beta_{arc,max}$. In that case, the loss will be distributed over a length $\Delta s = 2\sigma/x' \approx 11\text{m}$. A quench will therefore occur with a bunch intensity (case $\delta t < \tau_{metal}$ in Table 6)

$$n_q = 10^9 \Delta s = 10^{10} protons. \tag{26}$$

Table 6: Number of protons to induce a quench in the transient case at different time scales. A machine turn lasts $\tau_{turn} = 89\mu s$. Local losses happen at a step of the beam screen (upper half of the table). A distributed loss (lower half) over the length Δs can amount to $(dN/ds) \cdot \Delta s$. See table 2 for the sensitivity to the value of the critical temperature at top energy.

Time-scale	$\delta t < \tau_{\mathrm{metal}}$	$\delta t > \tau_{\mathrm{metal}}$	$\delta t \geq \tau_{\mathrm{He}}$	Min. Number of turns $\tau_{\mathrm{He}}/\tau_{turn}$
	Local losses N [protons]			
Injection	$1.0 \cdot 10^9$	$2.7 \cdot 10^9$	$2.5 \cdot 10^{10}$	500
Top Energy	$4.7 \cdot 10^5$	$8.5 \cdot 10^5$	$3.4 \cdot 10^7$	90
	Distributed losses dN/ds [protons/m]			
Injection	$1.0 \cdot 10^9$	$2.7 \cdot 10^9$	$2.5 \cdot 10^{10}$	500
Top Energy	$6.4 \cdot 10^5$	$1.2 \cdot 10^6$	$4.6 \cdot 10^7$	90

The intensity of the bunch shall therefore not be much larger than $\approx 3 \cdot 10^9$ protons.

5.2 A BATCH AT INJECTION

A batch is $\Delta t = 6\mu$s and thus $\Delta t < \tau_{metal}$. The quench limit for a distributed loss therefore remains the one discussed in Section 5.1, $n_q = 10^{10} protons$. The intensity of a batch is $n_{batch} = 2.5 \cdot 10^{13}$protons. The ratio of the two numbers indicates that the injection must be a very clean process. The transverse excursions of the injected beam must be limited by collimation in the warm transfer channel, leaving enough clearance between the edge of the beam and the beam screen, which shall in no circumstance scrape the beam directly. Obviously also, the collimators of the ring must be in operation during the injection process, to protect the machine against potential instabilities affecting either the injected or the already stored batches.

5.3 LOSSES AT THE BEGINNING OF THE RAMP

During the injection process, a finite fraction of the protons will end-up outside of the RF-buckets, or migrate there later, even in good operational conditions. This fraction is estimated to be of several percents. During the acceleration, these protons will drift towards the vacuum chamber and produce a flash of losses [22]. With the presently foreseen ramping curve [23], the flash shall last $\delta t \approx 0.2s < \tau_{He}$ or $\delta n_{turns} \approx 2000$. This is long enough to make use of the full reserve of heat of the helium in the cable. To allow for a strong fraction ($\sim 100\%$) of the injected beam to be outside the RF-buckets, the efficiency of the collimation system shall therefore be

$$r > \frac{N_{\mathrm{stored}}}{2.5 \cdot 10^{10} \cdot \Delta s} = \frac{3 \cdot 10^{14}}{2.5 \cdot 10^{11}} \approx 1200 \qquad (27)$$

Table 7: Rate of continuous local losses of protons per meter which induce a quench.

	$w_q[\mathrm{Wcm}^{-3}]$	$\dot{n}_q$
Injection	0.01	$7 \cdot 10^8 \mathrm{p}m^{-1}s^{-1} = 6.5 \cdot 10^4 \mathrm{p}m^{-1}turn^{-1}$
Top Energy	0.005	$7.8 \cdot 10^6 \mathrm{p}m^{-1}s^{-1} = 7 \cdot 10^2 \mathrm{p}m^{-1}turn^{-1}$

6 CONTINUOUS LOSSES , A REMINDER

A continuous heat deposit implies a continuous evacuation of heat to keep the temperature constant in the cables, and below the critical temperature. The limit of heat flow is set by the conduction of heat by the HeliumII flow through the insulation of the conductor, a mechanism which has no more to do with specific heat considerations. The present limits are set by the studies on the insulation of the cables made at Saclay [24]. The limit of heat transmission capability w_q (here reduced to a power evacuated out of the cable per unit volume) is reached and a quench occurs with the unit power deposition given in Table 7. The values of w_q might change with a different kind of insulation by a factor of two, more or less. The number of protons which can be lost locally per second in a continuous way must therefore be smaller than (see Table 1 for $\varepsilon_{\mathrm{ra,dist}}$)

$$\dot{n}_q = w_q / \varepsilon_{\mathrm{ra,dist}}. \tag{28}$$

ACKNOWLEDGEMENTS

The authors used with profit some intermediate results of the ongoing studies of Jean-Michel Depond. They had the benefit of the expertise of Prof. Martin Wilson, Jacques Gareyte and Philippe Lebrun.

References

[1] L.Burnod and D.Leroy, LHC Note 65,1987.
[2] A. van Ginneken, CASIM, Fermilab TN 309,1978.
[3] L. Burnod and J.B. Jeanneret, CERN SL/91-39(EA), LHC Note 167,1991.
[4] A. Fasso, private communication,1987.
[5] G.R. Stevenson and J.M. Zazula, CERN-TIS-RP/IR/92-30,1992.
[6] A.Fasso, A. Ferrari, J. Ranft, P. Sala, G.R. Stevenson and J.M. Zazula, FLUKA92,Workshop on Simulation of Accelerator Radiation Environments, Santa-Fe,1993.
[7] L. Burnod , J.B. Jeanneret and H. Schonbacher, CERN AC/DI/FA/Note 93-06,1993.
[8] J.M. Depond, LHC Note, to be issued.
[9] The LHC AcceleratorProject, CERN/AC/93-03(LHC), November 1993.
[10] The LHC Conceptual Design, CERN/AC/95-05(LHC), October 1995.
[11] P. Lebrun in CAS, CERN 89-04, S. Turner editor, March 1989.
[12] C. Schmidt, in Workshop on 'Stabilite des Supraconducteurs en Helium I et Helium II', Institut International du Froid editeur, 1981.
[13] C. Kittel, Introduction a la Physique du solide, Dunod editor, 1972.
[14] The Handbook of Chemistry and Physics,72nd edition, D.R.Lide editor,1991-1992,CRC Press.
[15] N.E. Phillips in Encyclopedia of Physics, Besancon editor, van Nostrand, 1974.
[16] S.A. Elrod,J.R. Miller and L. Dresner, Adv. Cryo.Eng, 28(1982)601.
[17] M.S. Lubell, IEEE Transactions on Magnetics,MAG-19,3(1983),754.
[18] B. Szeless, private communication, May 1996.
[19] H. Brechna, in Workshop on 'Stabilite des Supraconducteurs en Helium I et Helium II', Institut International du Froid editeur, 1981.
[20] R.D. McCarty, NBS Technical Note 1029.
[21] R.D. McCarty, NBS Technical Note 1972.
[22] J.B. Jeanneret, CERN/SL/Note 92-56(EA), October 1992.
[23] A. Faus-Golfe, LHC Project Note 9, May 1995.
[24] L. Burnod,D. Leroy,B. Szeless,B. Baudoy and C. Meuris, EPAC'94 London and CERN AT/94-21 (MA), LHC Note 281, August 1994.